
MARGINALIZED BEAM SEARCH ALGORITHMS FOR HIERARCHICAL HMMs

Xuechun Xu, Joakim Jaldén

EECS

KTH, Loyal Institution of Technology

Stockholm, Sweden

chunxxc@gmail.com, jalden@kth.se

ABSTRACT

Inferring a state sequence from a sequence of measurements is a fundamental problem in bioinformatics and natural language processing. The Viterbi and the Beam Search (BS) algorithms are popular inference methods, but they have limitations when applied to Hierarchical Hidden Markov Models (HHMMs), where the interest lies in the outer state sequence. The Viterbi algorithm can not infer outer states without inner states, while the BS algorithm requires marginalization over prohibitively large state spaces. We propose two new algorithms to overcome these limitations: the greedy marginalized BS algorithm and the local focus BS algorithm. We show that they approximate the most likely outer state sequence with higher performance than the Viterbi algorithm, and we evaluate the performance of these algorithms on an explicit duration HMM with simulation and nanopore base calling data.

Keywords Decoding · HHMM · Beam Search · Viterbi

1 Introduction

Many research fields require modelling the dependencies between a sequence of states $\hat{S}_{1:L} \triangleq \{\hat{S}_l\}_{l=1}^L$ and a sequence of observations $X_{1:T} \triangleq \{X_t\}_{t=1}^T$, where the state sequence length L is smaller than the observation sequence length T . Usually, the length difference implies that a variable number of consecutive observations depend on or are dominated by any one state \hat{S}_l . Example state and observation sequence pairs are words and speech signals in speech recognition [1, 2, 3, 4, 5], target activities and video frames in behavioural modelling [6, 7, 8, 9], or nucleotides and ion current measurements in nanopore base calling [10, 11, 12].

Hierarchical hidden Markov models (HHMMs) [13] have emerged as a common tool for modelling such scenarios. Referring to \hat{S}_l as the sequence-aligned state, the HHMM is built upon a hierarchy of time-aligned (observation-aligned) states S_t^r , where $r = 1, 2, \dots, R$ is the level (rank) in the hierarchy. Each level represents a specific temporal scale or abstraction level of the observations. We refer to the original state \hat{S}_l and the highest level state S_t^1 as the sequence- and time-aligned *outer state*, respectively, and require that \hat{S}_l and S_t^1 belong to the same state space $\mathbb{S} = \mathbb{S}^1$. The lower level states S_t^r for $r = 2, \dots, R$ are referred to as the *inner states* and belong to some, possibly different, individual state spaces \mathbb{S}^r . For convenience, we will use $S_t \triangleq (S_t^1, \dots, S_t^R)$ to denote the joint set of time-aligned states of all levels at time t . Under some additional constraints to be defined later, one can introduce a many-to-one (surjective) mapping from $S_{1:T} \triangleq \{S_t\}_{t=1}^T$ to $\hat{S}_{1:L}$ such that $\hat{S}_{l_t} = S_{l_t}^1$ for some sequence $\{l_t\}_{t=1}^T$ with $1 \leq l_t < l_{t+1} \leq L$. Essentially, the hierarchy of states allows the outer states to be aligned with the observations. With the time-aligned states, the Viterbi algorithm [14] provides a linear-time solution to

$$\operatorname{argmax}_{S_{1:T}} P(S_{1:T}|X_{1:T}) = \operatorname{argmax}_{S_{1:T}} P(S_{1:T}, X_{1:T}), \quad (1)$$

i.e., a way to infer the most likely state sequence over all levels of the hierarchy. However, inferring the most likely set of *sequence-aligned* outer states by solving

$$\operatorname{argmax}_{\hat{S}_{1:L}} P(\hat{S}_{1:L}|X_{1:T}) = \operatorname{argmax}_{\hat{S}_{1:L}} P(\hat{S}_{1:L}, X_{1:T}) \quad (2)$$

typically remains intractable due to the need for marginalizing over the set of $S_{1:T}$ that map to any $\hat{S}_{1:L}$. The problem in (2), which we will refer to simply as the *decoding* problem, is the key inference problem studied in this work.

Numerous studies have been dedicated to finding approximate solutions to the decoding problem since $\hat{S}_{1:L}$ is the main quantity of interest in applications such as speech recognition or nanopore sequencing. The alignment information in these applications is typically of secondary importance. This said, one viable approximate approach to this problem is to bypass the marginalization entirely, obtain $S_{1:T}$ by solving the inference problem in (1) using the Viterbi algorithm, and then promote the $\hat{S}_{1:L}$ mapped from such $S_{1:T}$ as a solution to the decoding problem. Projects using this approach have reported good performances [15, 16], despite the absence of any theoretical optimality guarantees in terms of (2). The same approach also extends to other graphic models, such as Bayesian network and conditional random field [17, 18], where the Viterbi is generalized into the max-product algorithm that can find the most-likely path along the graph.

Other approaches strive to account for the state hierarchy to achieve a better approximation by partially marginalizing over the set $S_{1:T}$ that maps to any $\hat{S}_{1:L}$. The surjective mapping from $S_{1:T}$ to $\hat{S}_{1:L}$ necessitates constraints on the inner states structure that explicitly marks the start/end of states at each level.¹ In [14], the authors introduce a binary indicator variable F_t^r , where $F_t^r = 1$ indicates the end of a state at a higher level $r - 1$ at time t , forcing a state transition, and $F_t^r = 0$ indicates the continuation of a state. Let $(S_{1:T}^1, F_{1:T}^2)$ denote the jointly time-aligned outer states and the second-order indicators. One can then in principle compute the marginal probability $P(S_{1:T}^1, F_{1:T}^2, X_{1:T})$ from summing $P(S_{1:T}, X_{1:T})$ over all $(S_{1:T}, F_{1:T})$ that maps to $(S_{1:T}^1, F_{1:T}^2)$, then $P(\hat{S}_{1:L}, X_{1:T})$ by summing $P(S_{1:T}^1, F_{1:T}^2, X_{1:T})$ over all $(S_{1:T}^1, F_{1:T}^2)$ that maps to $\hat{S}_{1:L}$. The Marginalized Viterbi algorithm (MVA) was developed in [19] to find the most likely outer state jointly with the indicators, i.e., $\operatorname{argmax}_{S_{1:T}^1, F_{1:T}^2} P(S_{1:T}^1, F_{1:T}^2, X_{1:T})$. The MVA is a re-discovery of the modified Viterbi algorithm of [16], designed to find the outer states with its ‘critical edges’, conceptually equivalent to the indicators $F_{1:T}^2$. The sequence $\hat{S}_{1:L}$ is then simply extracted from the MVA result $(S_{1:T}^1, F_{1:T}^2)$ and promoted as the decoding solution. It is proven in [16] that such $\hat{S}_{1:L}$ mapped from $(\hat{S}_{1:T}^1, F_{1:T}^2)$ is the optimal solution of the decoding problem in (2) only if the mapping is one-to-one (bijective), which is rarely realistic. Proper marginalization over $F_{1:T}^2$ generally remains intractable.

In this paper, we propose an alternative approach for decoding HHMMs that further marginalizes the ‘critical edges’ $F_{1:T}^2$ to approximately compute $\operatorname{argmax} P(\hat{S}_{1:L}, X_{1:T})$ in (1), instead of completely bypassing or only partially marginalizing. To achieve this, we extend the pruning-based Beam Search (BS) algorithm to the HHMM. In the following sessions, we first describe the inference methods available for general HHMMs. Then, we outline the fundamental principles behind applying the modified BS algorithms on HHMMs to find the approximated $\hat{S}_{1:L}$. Depending on the pruning approach selected, our proposal yields the Greedy Marginalized BS (GMBS) and the Local Focused BS (LFBS), with the latter having reduced complexity.

2 Hierarchical HHMMs

For simplicity of notation, we only consider $R = 2$ in the remainder of this work, i.e., $r \in \{1, 2\}$, because the principles are the same for hierarchies with $R > 2$. In order to achieve the surjective mapping from $S_{1:T}$ to $\hat{S}_{1:L}$ similar to the introduction of $F_{1:T}$ in [14], but with a more concise notation, we design the inner state space to consist of two subsets named the *end* and the *continuation* sets, denoted by \mathbb{S}_e^2 and \mathbb{S}_c^2 . If the inner state takes a value from the end subset, the current outer state is forced to end and will transit; otherwise, the outer state continues dwelling.² Figures 1 and 2 show an example of a rank 2 HHMM and its time-aligned representation. For simplicity of exposition, we define $\mathbb{S} \triangleq \{A, C, G, T\}$ and $\mathbb{S}^2 \triangleq \{1, \dots, |\mathbb{S}^2|\}$ for all examples in this paper, consistent with our benchmarking experiments using the nanopore base-calling dataset, where \mathbb{S} and \mathbb{S}^2 denote the nucleotide bases and an explicit duration variable, respectively, and let $\mathbb{S}_e^2 \triangleq \{1\}$ and $\mathbb{S}_c^2 \triangleq \{2, \dots, |\mathbb{S}^2|\}$.

Being an extension of HMMs, the HHMMs also assume the Markov property of all ranked states and the observations. Given $S_{1:t}$ and $X_{1:t}$, one can compute $P(S_{1:t}, X_{1:t})$ on the HHMM using the forward algorithm designed for plain HMMs by treating the joint states S_t as a (combined) hidden state. The joint probability $P(\hat{S}_{1:t}, X_{1:t})$ can, in principle but at considerable complexity, be computed by marginalizing $P(S_{1:t}, X_{1:t})$ over the set $\mathbb{B}_t(\hat{S}_{1:t})$ of sequences $S_{1:t}$

¹Otherwise, the mapping from $S_{1:T}$ to $\hat{S}_{1:L}$ is not proper. An example from nanopore base calling, where the states are the four nucleotides $\{A, C, G, T\}$, is that $S_{1:5}^1 = \{C, C, A, A, T\}$ can map to either $\hat{S}_{1:3} = \{C, A, T\}$ or $\hat{S}_{1:4} = \{C, A, A, T\}$ with $\hat{S}_2 = A$ ending at $t = 3$ or $t = 4$ alternatively.

²One can, for example, relate the end and the continuation subsets to F_t^2 by considering the end set as the joint state space $\mathbb{S}_e^2 = \{\mathbb{S}^2, F = 1\}$, and the continuation set as $\mathbb{S}_c^2 = \{\mathbb{S}^2, F = 0\}$ for some original inner state space \mathbb{S}^2 .

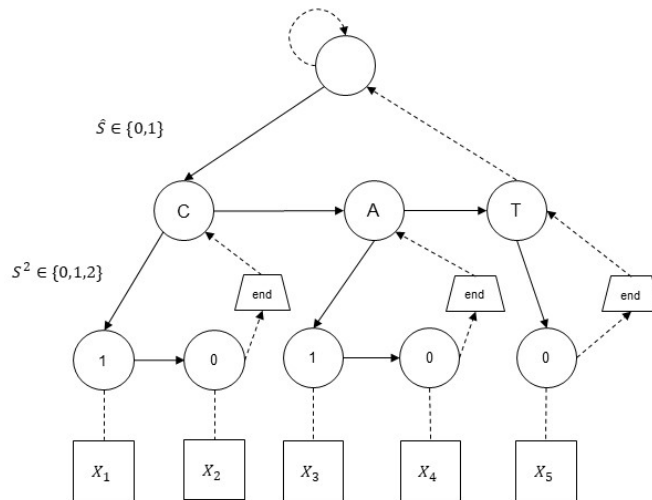


Figure 1: Illustration of a rank 2 HHMM with $\hat{s}_{1:3} = \{C, A, T\}$ and the inner states $\{1, 0\}$, $\{1, 0\}$ and $\{0\}$ dominated by each outer state respectively. We define $S_c^2 = \{0\}$ and $S_c^2 = \{1, 2\}$ as the end and continuation subset of the inner state space. The dashed arrow indicates when the lower level states end and forces transit in higher level states.

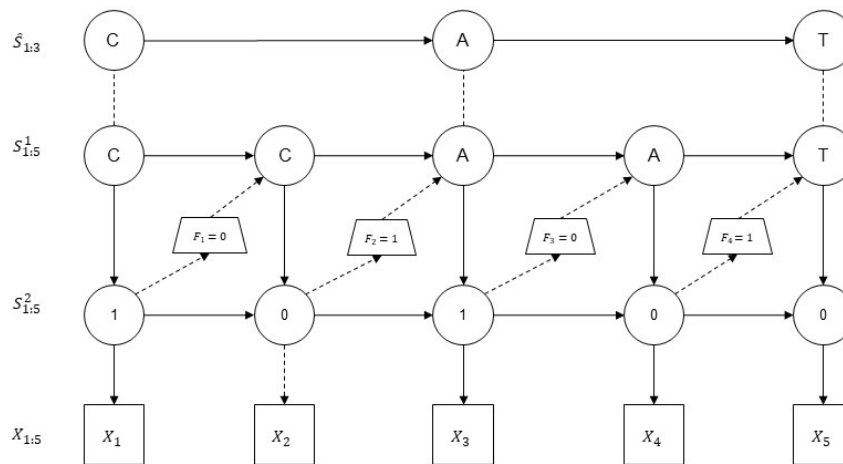


Figure 2: Illustration of a rank 2 time-alignment of the HHMM shown in Figure 1. It is reformed as the time-aligned outer states $S^1_{1:5} = \{C, C, A, A, T\}$ and inner states $S^2_{1:5} = \{1, 0, 1, 0, 0\}$. The indicators $F_2 = 1$ and $F_4 = 1$ identified the end of \hat{S}_1 at time 2 and \hat{S}_2 at time 4, which is equivalent to have $S_c^2 = \{0\}$ and $S_c^2 = \{0\}$, with end set defined as $S_c^2 = \{0\}$. Evidently, $F_t = 1$ whenever $S_t^2 \in S_c^2$.

that maps to the sequence-aligned outer state sequence $\hat{S}_{1:l}$, according to

$$P(\hat{S}_{1:l}, X_{1:t}) = \sum_{S_{1:t} \in \mathbb{B}_t(\hat{S}_{1:l})} P(S_{1:t}, X_{1:t}) \quad (3)$$

If we use $\chi_t(\hat{S}_{1:l}, i)$ to denote the joint probability of $X_{1:t}$ and $\hat{S}_{1:l}$ with its current inner state $S_t^2 = i \in \mathbb{S}^2$ at time t then, naturally, $P(\hat{S}_{1:l}, X_{1:t})$ can be rewritten using $\chi_t(\hat{S}_{1:l}, i)$ after marginalization over S_t^2 , i.e.,

$$P(\hat{S}_{1:l}, X_{1:t}) = \sum_{i \in \mathbb{S}^2} \chi_t(\hat{S}_{1:l}, i). \quad (4)$$

Combing (3) with (4) yields

$$\chi_t(\hat{S}_{1:l}, i) = \sum_{S_{1:t} \in \mathbb{B}_t(\hat{S}_{1:l}), S_t^2 = i} P(S_t = (\hat{S}_l, i), S_{1:t-1}, X_{1:t}),$$

where $\chi_t(\hat{S}_{1:l}, i)$ is computed as the sum over a subset of $\mathbb{B}_t(\hat{S}_{1:l})$ where the current inner state $S_t^2 = i$. It can be shown (see Appendix A for detailed proofs) that the probability $\chi_t(\hat{S}_{1:l}, i)$ can be computed recursively from χ_{t-1} as follows:

$$\begin{aligned} \chi_t(\hat{S}_{1:l}, i) &= \sum_{j \in \mathbb{S}^2} P\left(S_t = (\hat{S}_l, i), X_t | S_{t-1} = (\hat{S}_{l-1}, j)\right) \chi_{t-1}(\hat{S}_{1:l-1}, j) \\ &+ \sum_{k \in \mathbb{S}^2} P\left(S_t = (\hat{S}_l, i), X_t | S_{t-1} = (\hat{S}_l, k)\right) \chi_{t-1}(\hat{S}_{1:l}, k), \end{aligned} \quad (5)$$

in which the two terms represent two sources of the sequence $\hat{S}_{1:l}$ with a specific inner state i emerging at time t : the first term indicates that the sequence $\hat{S}_{1:l-1}$ existed at $t-1$ and extended a new outer state $S_t^1 = \hat{S}_l$ at time t , while the second term indicates the same sequence $\hat{S}_{1:l}$ that existed at $t-1$ and continued dwelling at time t . Marginalizing over the set $\mathbb{B}_t(\hat{S}_{1:l})$ entails recursively marginalizing over the two terms related to $\hat{S}_{1:l-1}$ and $\hat{S}_{1:l}$.

We can further simplify the model with the Markov assumption

$$P(S_t, X_t | S_{t-1}) = P(X_t | S_t, S_{t-1}) P(S_t | S_{t-1}) = P(X_t | S_t) P(S_t | S_{t-1}),$$

where $P(S_t | S_{t-1})$ is the HHMM transition probabilities, and $P(X_t | S_t)$ is the emission probability of observation X_t given the joint state $S_t = (S_t^1, S_t^2)$.³ On a hybrid construction of HHMMs and Neural Networks (NNs), the probability $P(X_t | S_t)$ may be replaced by a score $\phi(S_t | X_{t1:t2})$, which is the output of an NN assigned to the joint state S_t given a segment of observations as inputs [1, 11, 20, 21]. Finally, we achieve a recursive update of $\chi_t(\hat{S}_{1:l}, i)$ as

$$\begin{aligned} \chi_t(\hat{S}_{1:l}, i) &= P\left(X_t | S_t = (\hat{S}_l, i)\right) \left(\sum_{j \in \mathbb{S}^2} P\left(S_t = (\hat{S}_l, i) | S_{t-1} = (\hat{S}_{l-1}, j)\right) \chi_{t-1}(\hat{S}_{1:l-1}, j) \right. \\ &\quad \left. + \sum_{k \in \mathbb{S}^2} P\left(S_t = (\hat{S}_l, i) | S_{t-1} = (\hat{S}_l, k)\right) \chi_{t-1}(\hat{S}_{1:l}, k) \right). \end{aligned} \quad (6)$$

The likelihood of any given $(\hat{S}_{1:L}, S_T^2)$ and $X_{1:T}$ can, in principle, be computed by applying the recursion in (6) for $t = 1, \dots, T$. Together with (4), we can reformulate the decoding objective with χ_T as follows:

$$\hat{S}_{1:L}^* = \operatorname{argmax}_{\hat{S}_{1:L}, L \leq T} P(\hat{S}_{1:L}, X_{1:T}) = \operatorname{argmax}_{\hat{S}_{1:L}, L \leq T} \sum_{i \in \mathbb{S}^2} \chi_T(\hat{S}_{1:L}, i).$$

Ideally, one would obtain the optimal solution $\hat{S}_{1:L}^*$ by computing and sorting the likelihood $P(\hat{S}_{1:L}, X_{1:T})$ for all candidate sequences $\hat{S}_{1:L}$ and all $L \leq T$. However, this is computationally infeasible as the total number of candidates, i.e., $\sum_{1 \leq L \leq T} |\mathbb{S}|^L$, scales exponentially in T . Nevertheless, we can approximate $\hat{S}_{1:L}^*$ with tractable algorithms such as the BS algorithm, which only evaluates the recursion in (6) over a pruned candidate group. In the next chapter, we modify and generalize the standard BS algorithm to HHMMs.

³We use the first-order Markov assumption here for notational simplicity only. The argument is easily extended to higher-order Markov processes, and in the benchmark experiments described later, we assumed a fifth-order Markov chain, e.g., $P(S_t, X_t | S_{t-1}^2, \hat{S}_{l-4:l}) = P(X_t | \hat{S}_{l-4:l}) P(S_t | \hat{S}_{l-4:l})$ or $P(S_t, X_t | S_{t-1}^2, \hat{S}_{l-5:l-1}) = P(X_t | \hat{S}_{l-5:l-1}) P(S_t | \hat{S}_{l-5:l-1})$.

3 Marginalized Beam Search Algorithms

With the term ‘beam search’ first formalized in [22], the BS algorithm offers reduced computational complexity for decoding HMMs [23, 24] and conditional random fields [25, 26] compared to other well-known algorithms, such as the Viterbi algorithm. To achieve this, the BS optimizes a best-first search approach by maintaining a fixed beam-width W and tracking the W most likely state sequences, called *beams*, throughout the recursive forward search steps. At the start of each time step, the BS expands all possible next steps of each existing beam to create a set of *leaf beams*. Each leaf beam is assigned a score based on its parent beam and the current observation. The BS then sorts all leaf beams according to their scores and keeps the top- W as the new set of beams for the next step while pruning the rest. By recursively performing the expanding and pruning at each time step, the standard BS approximates the optimal solution of inference or decoding problems in a greedy manner.

However, in the context of decoding HHMMs, the BS requires an additional *marginalization* step before the pruning to maintain the recursive marginalization in (6). We refer to the BS algorithm with this additional step as the marginalized BS and introduce two variations based on different pruning steps in the following sections, the Greedy Marginalized BS and the Local Focused BS.

3.1 Greedy Marginalized Beam Search

The GMBS algorithm accommodates W beams, each capturing a *sequence-aligned* outer state sequence. We define $\mathbb{B}_{t-1}^{\text{BS}} \triangleq \{\hat{S}_{1:l_{t-1}^1}, \dots, \hat{S}_{1:l_{t-1}^W}\}$ to be the collection of candidate sequences captured at time $t-1$ by the W beams and denote the beams by $(\hat{S}_{1:l_{t-1}^w}, X_{1:t-1})$ for $w = 1, \dots, W$. At the beginning of time step t , the beams are expanded into a group of leaf beams that represent all possible next steps of $\mathbb{B}_{t-1}^{\text{BS}}$ in a union $\mathbb{B}_{t-1}^{\text{BS}} \cup \bar{\mathbb{B}}_t$. Specifically, the *extension* set $\bar{\mathbb{B}}_t$ is the collection of the sequences $\hat{S}_{1:(l_{t-1}^w+1)}$ for $w = 1, \dots, W$ created by extending a new outer state $\hat{S}_{(l_{t-1}^w+1)} \in \mathbb{S}$ at the end of $\hat{S}_{1:l_{t-1}^w}$, captured in the leaf beams $(\hat{S}_{1:(l_{t-1}^w+1)}, X_{1:t})$. Meanwhile, there are leaf beams $(\hat{S}_{1:l_{t-1}^w}, X_{1:t})$ that capture the same sequences $\hat{S}_{1:l_{t-1}^w} \in \mathbb{B}_{t-1}^{\text{BS}}$ as represented in the original W beams. We will refer to $\mathbb{B}_{t-1}^{\text{BS}}$ as the *continuation* set in contrast to the extension set.

Essentially, the extension and the continuation sets correspond to the two sources (i.e., sums) in (5) and (6). Therefore, given the scores of all existing beams at $t-1$, one can update the score of a specific leaf beam $(\hat{S}_{1:l}, X_{1:t})$ with any sequence $\hat{S}_{1:l} \in \mathbb{B}_{t-1}^{\text{BS}} \cup \bar{\mathbb{B}}_t$ analogously to (6) as

$$\begin{aligned} \bar{\chi}_t(\hat{S}_{1:l}) &= \sum_{i \in \mathbb{S}^2} \bar{\chi}_t(\hat{S}_{1:l}, i) \\ &= \sum_{i \in \mathbb{S}^2} P(X_t | S_t = (\hat{S}_l, i)) \left(\sum_{j \in \mathbb{S}_t^c} P(S_t = (\hat{S}_l, i) | S_{t-1} = (\hat{S}_{l-1}, j)) \bar{\chi}_{t-1}(\hat{S}_{1:l-1}, j) \right. \\ &\quad \left. + \sum_{k \in \mathbb{S}_t^c} P(S_t = (\hat{S}_l, i) | S_{t-1} = (\hat{S}_l, k)) \bar{\chi}_{t-1}(\hat{S}_{1:l}, k) \right), \end{aligned} \quad (7)$$

where we use the score $\bar{\chi}_t(\hat{S}_{1:l})$ and $\bar{\chi}_t(\hat{S}_{1:l}, i)$ to replace the probabilities $P(\hat{S}_{1:l}, X_{1:t})$ and $\chi_t(\hat{S}_{1:l}, i)$ respectively because they are not properly normalized due to the subsequent pruning step. As the GMBS algorithm operates on a pruned state space, it is possible that certain leaf beams may have both sources contained within the beams, while others may lack one of the sources, i.e., $\bar{\chi}_{t-1}(\hat{S}_{1:l-1}, j) = 0$ if $\hat{S}_{1:l-1} \notin \mathbb{B}_{t-1}^{\text{BS}}$ and $\bar{\chi}_{t-1}(\hat{S}_{1:l}, k) = 0$ if $\hat{S}_{1:l} \notin \mathbb{B}_{t-1}^{\text{BS}}$.

In the practical implementation, the computation of (7) is decomposed in two consecutive steps: expansion and marginalization. The expansion step is similar to the standard BS algorithm and involves computing scores of unmarginalized leaf beams, here referred to as the vanilla leaf beams, that capture the extension set $\bar{\mathbb{B}}_t$, and the continuation set $\mathbb{B}_{t-1}^{\text{BS}}$ separately, with $|\bar{\mathbb{B}}_t| = W|\mathbb{S}|$ and $|\mathbb{B}_{t-1}^{\text{BS}}| = W$. The score of the vanilla leaf beam representing $\hat{S}_{1:(l_{t-1}^w+1)} \in \bar{\mathbb{B}}_t$ is calculated by the first term in (7), i.e.,

$$\tilde{\chi}_t^c(\hat{S}_{1:(l_{t-1}^w+1)}) = \sum_{i \in \mathbb{S}^2} P(X_t | S_t = (\hat{S}_{(l_{t-1}^w+1)}, i)) \sum_{j \in \mathbb{S}_t^c} P(S_t | S_{t-1} = (\hat{S}_{l_{t-1}^w}, j)) \bar{\chi}_{t-1}(\hat{S}_{1:l_{t-1}^w}, j),$$

while the score of the vanilla leaf beam representing $\hat{S}_{1:l_{t-1}^w} \in \mathbb{B}_{t-1}^{\text{BS}}$ is calculated by the second term in (7), i.e.,

$$\tilde{\chi}_t^c(\hat{S}_{1:l_{t-1}^w}) = \sum_{i \in \mathbb{S}^2} P(X_t | S_t = (\hat{S}_{l_{t-1}^w}, i)) \sum_{k \in \mathbb{S}_t^c} P(S_t | S_{t-1} = (\hat{S}_{l_{t-1}^w}, k)) \bar{\chi}_{t-1}(\hat{S}_{1:l_{t-1}^w}, k).$$

The marginalization step then merges the vanilla leaf beams into a group of leaf beams representing the union $\mathbb{B}_{t-1}^{\text{BS}} \cup \bar{\mathbb{B}}_t$. It is important to note that the union size may be smaller, i.e., $|\mathbb{B}_{t-1}^{\text{BS}} \cup \bar{\mathbb{B}}_t| \leq W \times (1 + |\mathbb{S}|)$, due to the possible existence of redundant pairs of vanilla leaf beams representing two sources for the same leaf beam. The GMBS, therefore, needs to merge the redundant vanilla leaf beams into one leaf beam, which captures $\hat{S}_{1:l} \in \mathbb{B}_{t-1}^{\text{BS}} \cap \bar{\mathbb{B}}_t$ with a score that is the sum of the scored of the redundant vanilla leaf beams, i.e.,

$$\bar{\chi}_t(\hat{S}_{1:l}) = \tilde{\chi}_t^e(\hat{S}_{1:l}) + \tilde{\chi}_t^c(\hat{S}_{1:l}).$$

The non-redundant vanilla leaf beams are promoted directly to the leaf beams, inheriting the same score, i.e., $\bar{\chi}_t(\hat{S}_{1:l}) = \tilde{\chi}_t^c(\hat{S}_{1:l})$ for $\hat{S}_{1:l} \in \bar{\mathbb{B}}_t \setminus \mathbb{B}_{t-1}^{\text{BS}}$, and $\bar{\chi}_t(\hat{S}_{1:l}) = \tilde{\chi}_t^e(\hat{S}_{1:l})$ for $\hat{S}_{1:l} \in \mathbb{B}_{t-1}^{\text{BS}} \setminus \bar{\mathbb{B}}_t$. This merging step implicitly marginalizes over all possible ways of aligning the state sequences to the observations, albeit only over the set of possibilities represented by the kept beams.

However, finding the redundant vanilla leaf beams can pose a significant challenge in terms of both memory and computational resources, especially as the length l increases. Keeping all sequences in $\bar{\mathbb{B}}_t$ and \mathbb{B}_t^{BS} in memory and then comparing them individually is not a practical approach. In order to mitigate this issue, we propose an identifier (ID) based system, which will be discussed in the upcoming section. This system also ensures efficient marginalization.

After the expansion and the marginalization steps, the GMBS proceeds to perform the pruning step, which keeps only the top- W highest-scored leaf beams from among the leaf beams representing $\hat{S}_{1:l} \in \{\mathbb{B}_{t-1}^{\text{BS}} \cup \bar{\mathbb{B}}_t\}$:

$$\mathbb{B}_t^{\text{BS}} = \underset{\underbrace{\hat{S}_{1:l_1^t}, \dots, \hat{S}_{1:l_t^t}}_{\text{keep top-}W}}{\text{argmax}} \quad \bar{\chi}_t(\hat{S}_{1:l}) \quad \forall \hat{S}_{1:l} \in \{\mathbb{B}_{t-1}^{\text{BS}} \cup \bar{\mathbb{B}}_t\}.$$

The W surviving leaf beams are then promoted to the new set of beams representing \mathbb{B}_t^{BS} at time t , initiating the next step of the recursive loop.

3.1.1 Marginalization and Back-tracking with the ID System

The detection of redundant vanilla leaf beams is achieved by leveraging the commonality of their last outer state \hat{S}_l , and tracking back to the same ancestor beam that represents $\hat{S}_{1:l-1}$ at an earlier time. Despite storing and comparing the last state \hat{S}_l being a straightforward task, tracking the ancestor beams back in time can be challenging. We therefore propose an ID system that serves as a guidance mechanism to identify the common ancestor beam of redundant leaf beams in a computationally efficient manner.

During the expansion step at time t , each vanilla leaf beam is assigned an ID and a parent ID. More specifically, the vanilla leaf beam $(\hat{S}_{1:l}, X_{1:t})$ capturing the extension set $\hat{S}_{1:l} \in \bar{\mathbb{B}}_t$ is assigned a newly generated ID, which incorporates the current timestamp t , and a parent ID that is the ID of the beam $(\hat{S}_{1:l-1}, X_{1:t-1})$ from which it was expanded. Meanwhile, a vanilla leaf beam $(\hat{S}_{1:l}, X_{1:t})$ capturing the continuation set $\hat{S}_{1:l} \in \mathbb{B}_{t-1}^{\text{BS}}$ retains both the ID and the parent ID of the original beam $(\hat{S}_{1:l}, X_{1:t-1})$ without IDs being generated.

During the subsequent marginalization step, the algorithm first group all vanilla leaf beams by their parent IDs, which can be achieved efficiently by sorting the parent IDs. Then for the vanilla leaf beams sharing the same parent ID, the algorithm compares their last outer state to detect redundancies. Upon detection, the algorithm merges the redundant vanilla leaf beams into a new leaf beam with a score given by the sum of the vanilla leaf beams. It assigns the newly created leaf an ID according to the following rules: The resulting leaf beam retains both the ID and parent ID of the vanilla leaf beam capturing the continuation set, i.e., $\hat{S}_{1:l} \in \mathbb{B}_{t-1}^{\text{BS}}$, whose ID has the earlier timestamp. We illustrate the ID system in Figure 3 with an example for inferring a sequence {C, A, T} using the expansion and marginalization steps in the GMBS, leaving out the pruning step.

Crucially, the resulting leaf beam must carry the earlier timestamp ID to ensure the detection of redundant vanilla leaf beams in the future. Conversely, a redundant vanilla leaf beam capturing the extension set with the later timestamp (the current t) will not be the ancestor beam for any vanilla leaf beam at time $t + 1$; hence it would not be merged in any future step. Figure 4 demonstrates a case where redundancies are missed when the new leaf beam carries the later timestamp ID.

In the pruning step, the GMBS keeps the top- W leaf beams while maintaining their IDs, parent IDs and the last outer states. At time $t = T$, the GMBS performs a back-tracking procedure to reconstruct $\hat{S}_{1:L}$ with the help of the ID system. Starting with the most likely beam at time T , the GMBS traces back to its ancestor beam at a specific earlier time suggested by its parent ID, reversely concatenating their stored outer states. Then this procedure repeats, tracking the

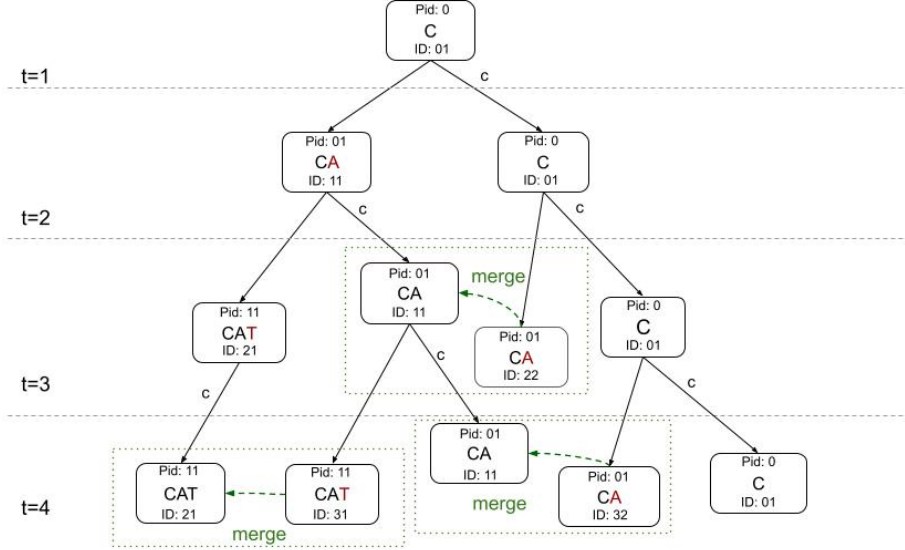


Figure 3: In this depiction, each vanilla leaf beam is represented as a rectangular shape, displaying its unique ID at the bottom and its parent ID (Pid) at the top. We use a two-digit ID, where the left digit is the timestamp and the right digit is unique for each vanilla leaf beam. The inner states have been omitted, and the Pid at $t = 0$ is fixed as 0. A small ‘c’ is put next to the arrow to indicate the continuation set. The temporal progression of the algorithm is exhibited for $t = 1, 2, 3$, shown in top-down order. At $t = 2$, two redundant vanilla leaf beams with ID 11 and ID 22 share the same Pid and last outer state; hence they are merged, preserving the ID 11 and the Pid 01. At $t = 3$, two pairs of redundant vanilla leaf beams are merged: those with ID 21 and ID 31 unite, preserving the ID 21 and Pid 11, and those with ID 11 and ID 32 merge, preserving the ID 11 and Pid 01. By $t = 3$, the GMBS generates three beams representing all possible sequence-aligned outer states of various lengths: $\{C\}$, $\{C, A\}$, and $\{C, A, T\}$. Note that the merging logic can be implemented only using the Pid and the last state, obviating the need for full sequence matching.

ancestor beams suggested by the parent IDs of the retrieved ancestor beams and concatenating their outer states until the parent ID timestamp is 0. Eventually, the sequence $\hat{S}_{1:L}$ is obtained by concatenating all stored outer states in the ancestor beams.⁴

The formalized approach of the GMBS is shown in Algorithm 1. With an infinite width W , the GMBS would compute the optimal decoding solution. Therefore, it is intuitive to select a large value of W . However, the GMBS entails sorting of up to $W \times (|\mathbb{S}| + 1)$ items, which has a time complexity of $\mathcal{O}(W|\mathbb{S}| \log(W|\mathbb{S}|))$ in a sequential implementation and of $\mathcal{O}(\log^2(W|\mathbb{S}|))$ in a parallel implementation assuming a parallel sorting algorithm such as a bitonic sorter [27]. The expansion step requires computing the probabilities over the inner states, i.e., computing χ_t in (5) for all $i \in \mathbb{S}^2$ and all beams, which has a time complexity of $\mathcal{O}(W|\mathbb{S}^2|^2)$ in a sequential implementation and of $\mathcal{O}(|\mathbb{S}^2|^2)$ in a parallel implementation. Therefore, the total time complexity of the sequential implementation is $\mathcal{O}(TW|\mathbb{S}^2|^2 + TW|\mathbb{S}| \log(W|\mathbb{S}|))$, and the time complexity of a parallel implementation with at least W threads is $\mathcal{O}(T|\mathbb{S}^2|^2 + T \log^2(W|\mathbb{S}|))$. To eliminate this costly sorting operation, we propose the LFBS algorithm that requires sorting only W lists, each of $|\mathbb{S}| + 1$ items.

3.2 Local Focus Beam Search

The LFBS provides a computationally efficient alternative to the GMBS, and involves the same expansion and marginalization step but a modified pruning step. With a fixed *focus-length* K , the LFBS algorithm maintains $M = |\mathbb{S}|^K$ beams at each step t . Each beam captures the most probable sequence that ends with a particular sequence of K consecutive outer states. In other words, the LFBS only focuses locally on the last K outer states of each candidate $\hat{S}_{1:l}$ via the implementation of the pruning step.

⁴Despite the timestamps carrying the meaning of a ‘critical edge’ when it is created, they are not the ‘critical edges’ for the retrieved $\hat{S}_{1:L}$ due to the marginalization step.

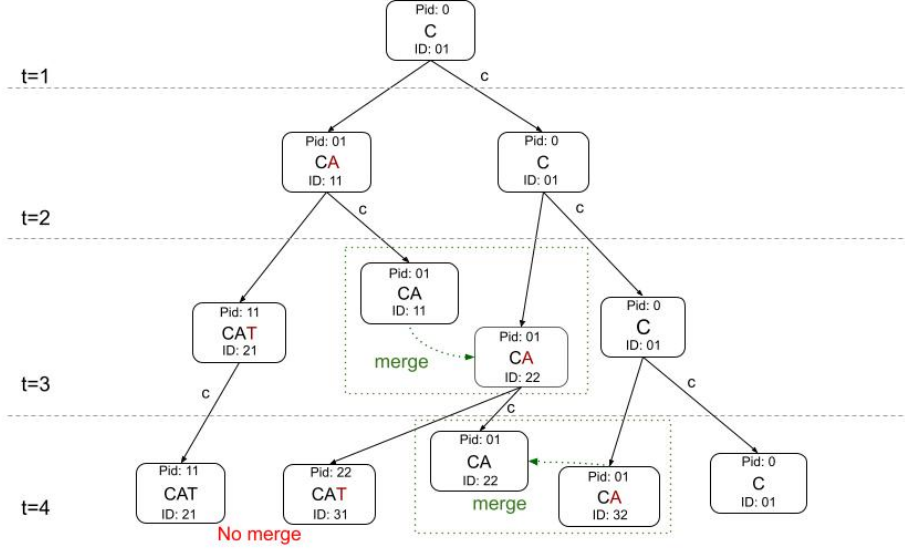


Figure 4: Illustration of missed detections of possible mergers when preserving the ID with the later timestamp in the same example shown in Figure 3. At $t = 2$, the leaf beam instead preserves ID 22. Consequently, at $t = 3$, the vanilla leaf beam with ID 31 has Pid 22, which is not the same Pid shared by its redundant vanilla leaf beam with ID 21. Therefore, the redundant pair, i.e., ID 21 and ID 31, can not be properly marginalized at time 3.

We denoted the m th beam at time $t - 1$ as $(\hat{S}_{1:l_{t-1}^m}, X_{1:t-1})$ for $m \in \{1, \dots, M\}$, such that $\hat{S}_{(l_{t-1}^m - K + 1):l_{t-1}^m} = A_m \in \mathbb{S}^K$. At the start of step t , the existing beams expand into leaf beams with scores computed by (7) using the same expansion and marginalization steps in the GMBS. When a vanilla leaf beam $(\hat{S}_{1:(l_{t-1}^m + 1)}, X_{1:t})$ is created at time t by extending the beam $(\hat{S}_{1:l_{t-1}^m}, X_{1:t-1})$ that existed at time $t - 1$, the LFBS ignores $\hat{S}_{l_{t-1}^m - K + 1}$ and shift the focus on the last K outer states of the new leaf beam, i.e., $\hat{S}_{(l_{t-1}^m - K + 2):(l_{t-1}^m + 1)} = A_n$ for certain $n \in \{1, \dots, M\}$.⁵ Here $n = m$ if the last $K + 1$ outer states $\hat{S}_{(l_{t-1}^m - K + 1):(l_{t-1}^m + 1)}$ are all identical. For any specific n and the sequence of K outer states A_n , there are $|\mathbb{S}|$ vanilla leaf beams ending with A_n , since there are $|\mathbb{S}|$ values of $\hat{S}_{l_{t-1}^m - K + 1}$. Including the one vanilla leaf beam created from continuing the original beam $(\hat{S}_{1:l_{t-1}^m}, X_{1:t-1})$, there are a total number of $|\mathbb{S}| + 1$ vanilla leaf beams capturing sequences ending with the same A_n . Moreover, as the beams encode their last K outer states with their index m , the indexes of the $|\mathbb{S}| + 1$ source beams for each n can be predetermined and remain the same throughout the algorithm. While this does not reduce the time complexity compared to a GMBS implementation with $W = M$ beams, it facilitates static memory allocations and access patterns for the list of beams and potentially large practical benefits in terms of run-time in an optimized software.

The expansion step results in M groups of vanilla leaf beams, such that the m th group captures $|\mathbb{S}| + 1$ sequences ending with the same K outer states A_m . Therefore, the LFBS only needs to verify redundant vanilla leaf beams within each group during the marginalization step and, similarly, perform the pruning step within each group afterwards. Specifically, during the pruning step, the LFBS algorithm sorts M lists of scores of all groups, each of which contains at most $|\mathbb{S}| + 1$ leaf beams, and then promotes the highest-scored one of the m th group to the m th beam in the time t while pruning the rest of the group, i.e.,

$$(\hat{S}_{1:l_t^m}, X_{1:t}) = \underset{(\hat{S}_{1:l}, X_{1:t})}{\operatorname{argmax}} \bar{\chi}_t(\hat{S}_{1:l}) \quad \forall \hat{S}_{(l-K+1):l} = A_m.$$

This modified pruning step of the LFBS returns M beams, each representing the most likely $\hat{S}_{1:l_t^m}$ ending with a specific A_m at time t . Figure 5 illustrates an implementation of the LFBS algorithm with the target sequence $\{A, C, C, A, T\}$.

In the end, by employing the same back-tracking strategy as in the GMBS, the LFBS reconstructs $\hat{S}_{1:L}$ as an approximation of the optimal decoding solution. The LFBS algorithm is formalized in Algorithm 2. Since the LFBS performs

⁵For example, both beams that end with $\{G, C, A\}$ and $\{A, C, A\}$ can expand to leaf beams that end with $\{C, A, T\}$ by dropping the first G or the first A, respectively, and extending with the T in the end.

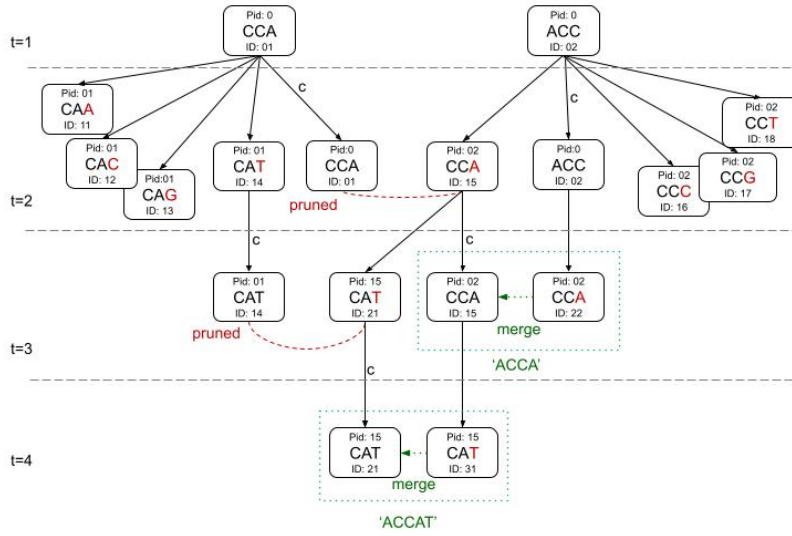


Figure 5: An implementation of the LFBS with $K = 3$, given the target sequence $\{A, C, C, A, T\}$. The inner state transitions and leaf beams with low scores are omitted in this illustration for simplicity. Only at $t = 1$ all vanilla leaf beams are listed: 5 vanilla beams from each original beam. At $t = 1$ the leaf beams with ID 01 (representing $\{C, C, A\}$) and ID 15 (representing $\{A, C, C, A\}$) both represent the last 3 outer states $\{C, C, A\}$. The LFBS prunes the leaf beam with ID 01 (assuming a lower score) and keeps the leaf beam with ID 15. At $t = 2$, the redundant leaf beams ID 15 and ID 22 (representing $\{A, C, C, A\}$) are detected and merged. In the following pruning step, the leaf beam with ID 21 is kept while the leaf beam with ID 14 is pruned. At $t = 3$, leaf beams with ID 21 and ID 31 are merged (representing $\{A, C, C, A, T\}$). In the end, the LFBS has computed $P(\{A, C, C, A, T\}, X_{1:3})$.

the marginalization and pruning within groups of size at most $|\mathcal{S}| + 1$, it does not face the problem of a costly sorting algorithm as in the GMBS. Combined with the expansion step, the total time complexity of the LFBS in a sequential implementation is $\mathcal{O}(TM|\mathcal{S}^2|^2 + T|\mathcal{S}| \log(|\mathcal{S}|))$, while in a parallel implementation is $\mathcal{O}(T|\mathcal{S}^2|^2 + T \log^2(|\mathcal{S}|))$. However, it requires $M = |\mathcal{S}|^K$ threads for parallel computing, each thread for a beam, which places a high demand on parallelism.

We end by pointing out that it follows directly by the analysis of Section 2 that both the GMBS and the LFBS become optimal solutions to the decoding as W and K , respectively, grow (very) large. The difference between the two marginalized BS algorithms lies in their respective strategies to select a small but representative subset of candidate beams at each recursion step to reach a given complexity budget. While the beams of the LFBS may not be as representative of the terms in (2) that contribute most to the overall score, the improved parallelism will practically allow for more beams at the same complexity. To assess the relative merits of the respective strategies, we turn next to empirical benchmarking experiments.

4 Benchmarking Experiments and Results

4.1 Benchmarking Experiments with the EDHMM

We conducted two experiments to assess the effectiveness and efficiency of the GMBS and LFBS algorithms in different scenarios. In the first experiment, we simulated the observation and the state sequences using an arbitrary explicit duration hidden Markov model (EDHMM) [28, 29], also referred to as Hidden semi-Markov models [30]. For the second experiment, we utilized the nanopore base calling dataset from our previous work on the Lokatt model, a hybrid model composed of an EDHMM and a neural network (NN) [11]. Both experiments involve the EDHMM, which contains an inner state known as the duration variable, denoted by d . This variable indicates the remaining time steps that an outer state will be dwelling on the time-aligned sequence, including the present time. The inner state space is therefore defined as $\{1, 2, \dots, D\}$, where D is the maximum (explicit) dwelling time, and can be divided into two subsets: the end subset $\mathbb{S}_e^2 = \{1\}$ and the continuation subset $\mathbb{S}_c^2 = \{2, 3, \dots, D\}$. By definition, d can only transit to $d - 1$ for $1 < d < D$ modelling a countdown to an outer transition, while $d = 1 \in \mathbb{S}_e^2$ forces an end to the outer state.

In our project, we also allowed the self-transition at $d = D$ such that the maximum dwell-time of the outer state can approach infinity with a geometrically decaying probability [11].

On the EDHMM, benchmarking against the Viterbi algorithm is equivalent to benchmarking against the MVA or the modified Viterbi algorithms. With the duration state, the mapping from the all-state sequences $S_{1:T}$ to $(S_{1:T}^1, F_{1:T}^2)$ is one-to-one (bijective). Thus computing $P(S_{1:T}^1, F_{1:T}^2)$, which required marginalizing over all $(S_{1:T}, F_{1:T})$ that maps to $(S_{1:T}^1, F_{1:T}^2)$, now equals computing $P(S_{1:T}, X_{1:T})$. Consequently, the decoding solution provided by the MVA [19], or the modified Viterbi algorithm in [16], is identical to the result obtained by the Viterbi algorithm applied directly to joint states of the HHMM [14].

We benchmarked the GMBS and LFBS against the Viterbi algorithm using various configurations in both experiments. Specifically, we implemented the GMBS with beam-width values of 8, 64, 256, and 512, while the LFBS was tested with focus-length values of 5, 6, and 7. All methods were implemented in a highly parallelized form on an NVIDIA V100 GPU card.

To assess the decoding performance, we measured the Levenshtein distance [31] between the decoding solution to a ground truth reference sequence. The Levenshtein distance is the minimal number of single-state edits (insertions, deletions or substitutions) required to change the former to the latter. The sequence accuracy, or the identity score in nanopore base calling, is the ratio of the number of matched outer states to the total number of alignment areas and is calculated as follows:

$$\text{accuracy} = \frac{\text{matches}}{\text{matches} + \text{mismatches} + \text{insertion} + \text{deletions}}.$$

We define the alignment area to begin at the first matched state and to end at the last matched state, to handle the base calling dataset where the reference is the entire genome (approximately 5 millions nucleotides) and is much longer than the reads [11].

In addition, we also reported decoding performances on areas consisting of k consecutive identical outer states, referred to as the ' k -mer homopolymers (HPs)' borrowed from the bioinformatics literature. Decoding these HPs has long been recognized as challenging for many decoding methods, especially in base calling projects where the HPs have random dwelling times and share nearly identical measurements among their component bases. We assessed HP decoding performance in terms of the number of correctly decoded HPs and the number of HPs covered in the mapped reference area, as well as their ratio as the accuracy. All codes and data used in the experiments can be found at the MBS git repository: <https://github.com/chunxxc/MBS.git>.

4.2 Simulation Experiment and Results

In the simulation experiment, we designed the outer states space to be $\mathbb{S} = \{A, C, G, T\}$ and the duration variable to have a Poisson distribution for $d \leq D$ and a geometric tail distribution with a fixed rate for $d > D$. The mean value for the Poisson distribution was set to 9, D was set to 16, and the fixed rate for the exponential distribution was set to 0.5625. The transition probability used in the base calling experiment, which was estimated using maximum likelihood estimation, or frequency count, from the reference genome, was utilized for generating $\hat{S}_{1:L}$. For each given reference length L ranging from 500 to 8000, 200 samples were generated by random sampling from the pre-obtained transition probability. Gaussian emission probabilities were used, where the observations were assumed to be a fifth-order Markov chain and were independent of duration variables, i.e., $P(X_t | \hat{S}_{t-4:t}) \sim \mathcal{N}(m_i, \sigma)$ for $i \in \{1, \dots, 4^5\}$. To facilitate comparisons of emission probabilities, we plotted the mean values of the Gaussian emission probabilities against all possible combinations of the five outer states in Figure 6. Standard deviations of the Gaussian emission probabilities were set to 2 and 4, respectively, to create scenarios of low and high noise ratios.

We used the PairwiseAligner function from Biopython packages [32] to align the reference and decoded outer state sequence.

4.2.1 Results

The mean values of the sequence accuracy for low and high emission noise scenarios are presented in Table 1 and 2, respectively. A clear trend of increasing accuracy with increasing sequence length is observed. Tables 3 and 4 report the average number of matched outer states in the low and high noise scenarios. All methods naturally show a reduced performance with increased noise levels, as evidenced by decreased accuracy and fewer matched states.

The GMBS and the LFBS outperform the Viterbi algorithm in low and high noise scenarios. Specifically, the Viterbi gives the least number of matched states since it is prone to favor shorter lengths as they have a higher probability resulting from less frequent state transitions. In contrast, the modified BS algorithms with the marginalization step are less discriminative over the lengths of candidates. The GMBS generally achieves higher sequence accuracy and

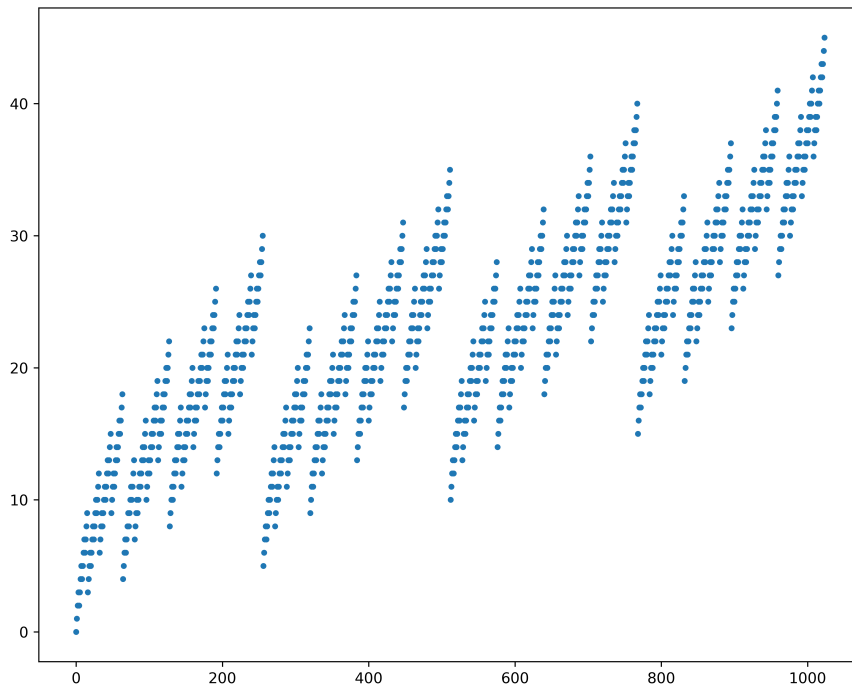


Figure 6: Mean values of the Gaussian emission probabilities used in the simulation experiments. The mean values are aligned according to the five consecutive outer state variations, indexed from 0 to 1023. The indexes are created by mapping $\{A, C, G, T\}$ to $\{0, 1, 2, 3\}$ and viewing the five mapped numbers as a base-4 number system starting with the left-most position, e.g. ‘CAAAA’ maps to 10000 and is indexed 1; ‘TTTTT’ maps to 33333 and is indexed 1023. The mean values are generated by multiplying a kernel $\{1, 2, 3, 4, 5\}$ with the five mapped numbers as a vector.

more matched outer bases than the LFBS. For both the GMBS and LFBS, a larger value of the beam width and the focus-length yields better performance, as expected. However, the performance gain becomes marginal as the computational cost grows. In particular, the improvement when increasing the beam width W from 8 to 64 is most significant. Meanwhile, the GMBS with beam width 8 displays a sign of degeneracy, which is comparable to the Viterbi and worse than the LFBS under the low noise scenario.

The decoding performances on the k -mer HPs are extracted from decoding results with reference lengths 1500 and reported in Table 5 and 6 under the low and high noise scenarios, respectively. The results are clustered with respect to the lengths of the homopolymers, where the difficulty of correctly decoding rises as the length grows. In addition, since the data were created with a fifth-order Markov assumption, the HPs longer than 5 are harder to decode. Similar to what is reflected in the decoding performances, the GMBS and the LFBS outperform the Viterbi in decoding HPs. A key point to consider is that the LFBS can not decode HPs longer than its focus-length K . The beams in the LFBS capturing various lengths of HPs were grouped together because they share the same last K outer states, among which, later in the pruning step, the longer ones were pruned due to lower probability from more state transitions. Nevertheless, the LFBS gives the most numbers for the HPs of length less than K and the highest overall accuracy for all HPs of length at least 3.

The last Table 7 presents the average decoding times per data for each method. For the GMBS, the number of logical threads issued per CUDA block [33] equals the chosen beam width: 8, 64, 256 and 512. For the LFBS, the number of logical threads issued are 4^K : 1024 for $K = 5$, 4096 for $K = 6$ and 16384 for $K = 7$. However, each physical thread on the GPU executes several logical threads because of the hardware limitation of at most 1024 threads per block and limits due to register memory on the GPU. Despite the exponential growth of the number of logical threads in the LFBS, the time cost of the LFBS scales almost linearly with respect to the focus-length K , similarly to the GMBS to

the beam-width W . However, despite the theoretical advantages, the LFBS takes longer to finish in practice, most likely due to a memory I/O bottleneck on the GPU. This may, however, change on an implementation on dedicated hardware.

Table 1: Mean sequence accuracy with emission standard deviation 2

Ref Length	1000	1500	2000	3000	4000	5000	6000	7000	8000
GMBS(8)	0.9602	0.9604	0.9617	0.9619	0.9620	0.9625	0.9626	0.9630	0.9631
GMBS(64)	0.9695	0.9695	0.9705	0.9701	0.9707	0.9711	0.9710	0.9713	0.9714
GMBS(256)	0.9703	0.9707	0.9713	0.9709	0.9715	0.9720	0.9717	0.9721	0.9722
GMBS(512)	0.9707	0.9709	0.9715	0.9711	0.9717	0.9722	0.9718	0.9722	0.9724
LFBS(5)	0.9641	0.9654	0.9666	0.9662	0.9664	0.9669	0.9664	0.9672	0.9673
LFBS(6)	0.9660	0.9671	0.9683	0.9678	0.9684	0.9689	0.9682	0.9691	0.9691
LFBS(7)	0.9666	0.9674	0.9687	0.9682	0.9688	0.9693	0.9686	0.9694	0.9695
Viterbi	0.9592	0.9608	0.9615	0.9618	0.9627	0.9630	0.9629	0.9628	0.9631

Table 2: Mean sequence accuracy with emission standard deviation 4

Ref Length	1000	1500	2000	3000	4000	5000	6000	7000	8000
GMBS(8)	0.7575	0.7603	0.7609	0.7616	0.7618	0.7624	0.7617	0.7626	0.7617
GMBS(64)	0.7740	0.7749	0.7755	0.7758	0.7762	0.7771	0.7767	0.7774	0.7759
GMBS(256)	0.7753	0.7756	0.7762	0.7767	0.7767	0.7778	0.7771	0.7780	0.7767
GMBS(512)	0.7753	0.7754	0.7762	0.7763	0.7769	0.7780	0.7772	0.7781	0.7768
LFBS(5)	0.7404	0.7410	0.7413	0.7431	0.7426	0.7436	0.7430	0.7435	0.7426
LFBS(6)	0.7436	0.7443	0.7440	0.7457	0.7459	0.7458	0.7456	0.7466	0.7457
LFBS(7)	0.7438	0.7453	0.7439	0.7462	0.7464	0.7467	0.7468	0.7473	0.7466
Viterbi	0.7106	0.7117	0.7120	0.7122	0.7129	0.7131	0.7127	0.7133	0.7134

Table 3: Average number of matched outer states with emission standard deviation 2

Ref Length	1000	1500	2000	3000	4000	5000	6000	7000	8000
GMBS(8)	982	1473	1965	2948	3932	4916	5901	6883	7869
GMBS(64)	987	1480	1971	2962	3947	4933	5925	6916	7904
GMBS(256)	988	1481	1972	2962	3948	4934	5925	6916	7906
GMBS(512)	988	1483	1973	2963	3950	4937	5929	6919	7910
LFBS(5)	987	1479	1970	2956	3943	4930	5918	6909	7893
LFBS(6)	987	1481	1971	2959	3950	4935	5926	6916	7906
LFBS(7)	988	1482	1972	2958	3950	4935	5929	6916	7907
Viterbi	974	1462	1944	2923	3903	4871	5851	6828	7805

Table 4: Average number of matched outer states with emission standard deviation 4

Ref Length	1000	1500	2000	3000	4000	5000	6000	7000	8000
GMBS(8)	859	1291	1722	2585	3447	4312	5172	6037	6895
GMBS(64)	882	1316	1751	2614	3509	4384	5232	6137	7004
GMBS(256)	882	1315	1751	2616	3517	4397	5240	6144	7011
GMBS(512)	882	1318	1753	2618	3517	4400	5247	6151	7024
LFBS(5)	876	1311	1746	2602	3494	4376	5224	6111	6982
LFBS(6)	880	1314	1748	2610	3508	4384	5228	6128	7004
LFBS(7)	881	1315	1745	2614	3506	4382	5235	6135	6992
Viterbi	810	1218	1630	2424	3253	4083	4857	5678	6463

4.3 Base Calling Experiment and Results

In the second experiment, we used the Lokatt model and data batch 2 from [11]. The dataset comprises raw reads (ion current measurements) generated by ONT MinION devices with the 1D protocol[10], and their corresponding Ecoli genome (nucleotide bases) as the reference sequence. The hybrid Lokatt model includes an EDHMM that employs the output of an NN in place of the emission probabilities. The pre-trained NN takes a raw read $X_{1:T}$ as input and generates

Table 5: Decoding performances on homopolymers with ref length 1500 and emission standard deviation 2

Methods	3-mer	4-mer	5-mer	6-mer	7-mer	8-mer	9-mer	Accuracy
GMBS(8)	9799/10482	2653/2884	816/908	197/254	38/54	7/11	4/8	0.9256
GMBS(64)	9960/10499	2690/2884	824/909	199/254	38/54	7/11	4/8	0.9387
GMBS(256)	9960/10505	2693/2885	824/909	199/254	39/54	7/11	4/8	0.9385
GMBS(512)	9965/10505	2695/2885	824/909	199/254	39/54	7/11	4/8	0.9390
LFBS(5)	9996/10497	2713/2888	825/909	0/254	0/53	0/11	0/8	0.9258
LFBS(6)	10008/10500	2723/2888	818/909	197/255	0/53	0/11	0/8	0.9400
LFBS(7)	10016/10500	2724/2887	818/909	198/254	37/54	0/11	0/8	0.9433
Viterbi	9672/10493	2640/2885	776/909	139/254	21/54	3/11	1/8	0.9069

*Results are displayed as numbers of ‘correctly-decoded/total homopolymers’.

Table 6: Decoding performances on homopolymers with ref length 1500 and emission standard deviation 4

Methods	3-mer	4-mer	5-mer	6-mer	7-mer	8-mer	9-mer	Accuracy
GMBS(8)	6665/10381	1750/2822	572/887	144/248	31/70	8/17	3/4	0.6357
GMBS(64)	6920/10398	1853/2822	605/888	146/247	33/70	10/17	4/4	0.6625
GMBS(256)	6900/10397	1858/2819	612/890	146/247	33/70	9/17	4/4	0.6620
GMBS(512)	6910/10406	1865/2822	612/890	147/247	33/70	10/17	4/4	0.6628
LFBS(5)	6907/10353	1875/2817	559/887	0/247	0/70	0/17	0/4	0.6489
LFBS(6)	6947/10359	1912/2815	579/886	126/249	0/69	0/17	0/4	0.6642
LFBS(7)	7000/10371	1924/2817	595/888	138/248	36/70	0/17	0/4	0.6724
Viterbi	6075/10216	1694/2788	514/877	108/244	16/70	4/17	1/4	0.5917

*Results are displayed as numbers of ‘correctly-decoded/total homopolymers’.

Table 7: Mean time cost (seconds)

Ref Length	1000	1500	2000	3000	4000	5000	6000	7000	8000
GMBS(8)	0.4120	0.6158	0.8043	1.1726	1.5888	1.9413	2.3157	2.7226	3.1338
GMBS(64)	0.9067	1.3523	1.7986	2.6936	3.5958	4.4971	5.4072	6.2591	7.2820
GMBS(256)	2.9821	4.4884	5.9852	8.9905	11.9829	15.0802	18.0231	21.1296	24.0776
GMBS(512)	6.3481	9.6344	12.8240	19.2897	25.5928	32.1701	38.5581	44.8304	51.4094
LFBS(5)	0.7342	1.105	1.4660	2.2106	2.9409	3.6768	4.4093	5.1546	5.8806
LFBS(6)	2.7459	4.1234	5.5016	8.2658	11.0160	13.8055	16.5822	19.3067	22.0654
LFBS(7)	11.1187	16.5055	22.0554	33.0467	43.7554	53.9086	70.2276	77.7335	90.3488

the sequence of likelihoods for 5 consecutive bases, referred to as 5-mers. The duration variable was set to follow a log-logistic distribution with an geometric tail, which was estimated with respect to each raw read based on the number of changes above a threshold level in the current amplitudes.

We used the software Minimap2 [34] to map the decoded outer states to the reference genome. The reads were selected into two categories, *short reads* and *long reads*, corresponding to lengths of 1000 – 2000 and 4000 – 5000 bases, respectively. To account for the random noise in the dataset, we evaluated the identity and number of matched bases in terms of both their means and medians.

4.3.1 Results

The results of the decoding experiment with short reads and long reads are reported in Table 8 and 9, respectively. We observe a slight decrease in the mean identity scores of all methods as the length increases, contrary to what was observed in the simulation experiment. This is likely due to the systematic errors in the devices, such as the ratcheting motor protein controlling the sequencing speed, leading to slightly lower quality measurements in long reads.

Although the modified BS algorithms demonstrated superior performance over the Viterbi algorithm in our simulation experiments, these benefits did not always remain when applied to a real-world base calling dataset. In particular, the Viterbi algorithm’s performance is comparable to the GMBS and the LFBS, even at their maximum configurations. The outstanding behavior of the Viterbi algorithm has been observed in previous reports based on real datasets, such as those in [15, 17, 18]. A possible explanation is the Lokatt model does not precisely match the underlying data-generating process of the base calling dataset. This mismatch may cause the additional marginalization step to contribute to incorrect predictions of the states. Nevertheless, all methods’ mean and median identity scores exhibited only minor

variations. The LFBS with focus-length 6 and 7 decoded the highest number of bases with a leading identity score in both cases.

The decoding performances of the homopolymers are presented in Table 10 and 11. The long HPs in the base calling dataset are harder to decode, resulting in all methods having lower performance than in the simulation experiments. In contrast to the identity scores, the marginalized BS algorithms outperform the Viterbi in decoding HPs of various lengths. The Viterbi typically has the least number of HPs correct and fails to decode homopolymers longer than 5. The GMBS with 512 beams shows superior performance regarding the number of correctly called HPs and overall accuracy. The LFBS, which can not decode HPs longer than the chosen K , caught up with the GMBS for decoding long HPs as the values of K increased.

Table 8: Decoding performances with short reads

Methods	Identity	Bases per read	Reads	Matched Bases
GMBS(8)	0.9141/0.9269	1669/1805	455	759781
GMBS(64)	0.9152/0.9303	1672/1816	458	765812
GMBS(256)	0.9161/0.9307	1679/ 1818	456	765411
GMBS(512)	0.9167 /0.9309	1681 /1817	455	765048
LFBS(5)	0.9154/ 0.9312	1671/1811	459	766902
LFBS(6)	0.9156/0.9311	1671/1811	459	767012
LFBS(7)	0.9159/ 0.9312	1675/1812	458	767060
Viterbi	0.9158/ 0.9312	1671/1810	458	765634

*Identity and the number of matched bases per read are listed as ‘mean/median’.

Table 9: Decoding performances with long reads

Methods	Identity	Bases per read	Reads	Matched Bases
GMBS(8)	0.9102/0.9277	4193/4504	544	2281135
GMBS(64)	0.9111/0.9298	4206/4510	546	2296959
GMBS(256)	0.9115/0.9305	4215/4510	546	2301715
GMBS(512)	0.9112/0.9299	4217/ 4514	546	2302800
LFBS(5)	0.9121/0.9311	4210/4513	547	2303138
LFBS(6)	0.9123/0.9315	4223 /4512	546	2306013
LFBS(7)	0.9124 /0.9315	4223 /4513	546	2305796
Viterbi	0.9122/ 0.9318	4216/4509	546	2302418

*Identity and the number of matched bases per read are listed as ‘mean/median’.

Table 10: Decoding performances on homopolymers with short reads

Methods	3-mer	4-mer	5-mer	6-mer	7-mer	8-me	Accuracy
GMBS(8)	3248/3966	717 /1047	145/320	5/91	0/23	0/10	0.7542
GMBS(64)	3286/3998	716/1054	146/323	6 /91	0/23	0/10	0.7555
GMBS(256)	3288/4005	717 /1054	148 /323	6 /91	0/23	0/10	0.7555
GMBS(512)	3276/3975	715/1049	148 /321	6 /91	0/23	0/10	0.7580
LFBS(5)	3290/4008	701/1054	132/323	0/91	0/23	0/10	0.7485
LFBS(6)	3292 /4008	710/1054	138/323	3/91	0/23	0/10	0.7522
LFBS(7)	3291/4008	711/1054	139/323	5/91	0/23	0/10	0.7527
Viterbi	3271/3977	699/1049	133/320	0/91	0/23	0/10	0.7502

*Results are displayed as numbers of ‘correctly-decoded/total homopolymers’.

5 Conclusion

In this paper, we have proposed the GMBS and the LFBS algorithms to approximate the solution for decoding the outer state sequences on a given HHMM. Our investigation into the performance of the two marginalized BS algorithms in simulated and real-world datasets has shown that they can outperform the Viterbi in certain scenarios. However, the advantages are insignificant when applied to real-world datasets, despite the Viterbi achieving fewer matched bases. The GMBS and the LFBS did not provide greater identity scores but generally matched more bases.

We also observed that the performance of different algorithms varies depending on the type of sequences being decoded, such as homopolymers of different lengths. The Viterbi has performed worse in terms of accuracy and numbers than the

Table 11: Decoding performances on homopolymers with long reads

Methods	3-mer	4-mer	5-mer	6-mer	7-mer	8-mer	9-mer	Accuracy
GMBS(8)	13293/16022	3042/4224	652 /1338	23 /369	1/72	0/23	0/2	0.7715
GMBS(64)	13363/16046	3044/4225	649/1337	23 /369	2 /72	0/23	0/2	0.7738
GMBS(256)	13363/16027	3045/4225	647/1336	23 /368	2 /73	0/23	0/2	0.7745
GMBS(512)	13380 /16037	3047 /4231	650/1338	23 /369	2 /73	0/23	0/2	0.7748
LFBS(5)	13370/16037	2994/4226	601/1335	0/368	0/73	0/23	0/2	0.7689
LFBS(6)	13375/16037	3026/4225	630/1336	13/368	0/73	0/23	0/2	0.7725
LFBS(7)	13371/16037	3027/4225	635/1336	21/368	2/73	0/23	0/2	0.7731
Viterbi	13328/16029	2989/4226	585/1335	0/368	0/73	0/23	0/2	0.7664

*Results are displayed as numbers of ‘correctly-decoded/total homopolymers’.

GMBS and the LFBS in decoding homopolymers. Moreover, the computational cost of the GMBS and the LFBS in a parallel implementation increased linearly with their parameter value, though are still more costly than the Viterbi. When choosing the decoding algorithm, one must therefore consider the trade-off between accuracy and speed.

These findings provide insights into the selection and optimization of BS algorithms in base calling applications and may guide future research in this area. However, our study has some limitations. Our analysis was based on a specific base calling dataset and may not generalize to other datasets with different characteristics, such as natural language datasets. Future work could expand the scope of the study by testing more algorithms and evaluating their performance on different datasets. Additionally, it would be interesting to explore the effect of parameter tuning on the performance of the BS algorithms, as well as the potential benefits of combining different algorithms or developing novel hybrid methods.

Last but not least, the two BS algorithms proposed in this work are also, in principle, applicable to graphic models without explicit Markov properties, such as the Connectionist Temporal Classification (CTC) graphs [35]. We will, however, leave the exploration of this to future work.

Acknowledgments

The authors acknowledge support from Patrik Ståhl and Nayanika Bhalla, and the National Genomics Infrastructure (NGI) in Stockholm. This work has been supported by the Swedish Research Council Research Environment Grant QuantumSense [VR 2018-06169].

Algorithm 1 The GMBS algorithm

```

1: Input:  $X_{1:T}$ , HHMM,  $W$ 
2: Output: the sequence  $\hat{S}_{1:L}$ 
3: Initialise with priors  $P(\hat{S})$ 
4: At  $t = 1$ 
5: 1. Create leaf beams  $(\hat{S}_1, X_1)$  for all  $\hat{S}_1 \in \mathbb{S}$  and
6: 2. assign each a score  $P(\hat{S}_1, X_1) = P(X_1|\hat{S}_1)P(\hat{S}_1)$ .
7: 3. Sort and keep the top- $W$  highest-scored leaf beams as the beam.
8: 4. Assign a unique ID with timestamp  $t$  to each beam.
9: for  $t = 2, \dots, T$  do
10:   procedure EXPANDING
11:     for Every beam  $(\hat{S}_{1:l_{t-1}^w}, X_{1:t-1})$  (in parallel) : do
12:       1. Expand  $|\mathbb{S}|$  vanilla leaf beams  $(\hat{S}_{1:(l_{t-1}^w+1)}, X_{1:t})$  and compute their scores, and
13:       2. assign each a unique ID with timestamp  $t$ , with the ID of the original beam as their parent ID.
14:       3. Expand a vanilla leaf beam  $(\hat{S}_{1:l_{t-1}^w}, X_{1:t})$ , compute its score, and
15:       4. maintain the same ID and the same parent ID of the original beam.
16:     end for
17:   end procedure
18:   procedure MARGINALIZING
19:     1. Sort the parent ID of all vanilla leaf beams, and
20:     2. for these sharing the same parent ID, check if they also share the same last state
21:     3. Merge the redundant vanilla leaf beams as described in Chapter 3.1.1.
22:     4. Promote the non-redundant vanilla leaf beams as leaf beams.
23:   end procedure
24:   procedure PRUNING
25:     1. Sort remaining leaf beams by their scores.
26:     2. Promote the top- $W$  leaf beams to the beams  $(\hat{S}_{1:l_t^w}, X_{1:t})$ .
27:   end procedure
28: end for
29: procedure BACKWARDS-TRACKING
30: 1. Select the highest-scored beam  $(\hat{S}_{1:l_T^w}, X_{1:T}) = \operatorname{argmax} \bar{\chi}_T(\hat{S}_{1:l_T^w})$ .
31: 2. Back trace to the ancestor beam pinpointed by the parent ID of the selected beam.
32: 3. Concatenating the recorded last outer states in the parent beam.
33: 4. If the timestamp in the parent ID is 0, end the procedure, otherwise,
34: 5. make the parent beam the selected beam and return to 2.
35: end procedure

```

Algorithm 2 LFBS algorithm

```

1: Input:  $X_{1:T}$ , HHMM,  $K$ ,  $M = |\mathbb{S}|^K$ 
2: Output:  $\hat{S}_{1:L}$ 
3: Initialise with priors  $P(A_m)$  for  $m = 1, \dots, M$ 
4: At  $t = 1$ 
5: 1. Create  $M$  beams  $(\hat{S}_{1:K}, X_1)$  for all  $\hat{S}_{1:K} = A_m \in \mathbb{S}_{1:K}$  and
6: 2. assign  $m$ th beam a score  $P(A_m, X_1) = P(X_1|A_m)P(A_m)$ .
7: 3. Assign a unique ID with timestamp  $t$  to each beam.
8: for  $t = 2, \dots, T$  do
9:   procedure EXPANDING
10:   for the  $m$ th beam  $(\hat{S}_{1:t-1}^m, X_{1:t-1})$  (in parallel) do
11:     1. Expand  $|\mathbb{S}|$  vanilla leaf beams  $(\hat{S}_{1:(t-1)+1}^m, X_{1:t})$  and compute their scores, and
12:     2. assign each a unique ID with timestamp  $t$ , with the ID of the original beam as their parent ID.
13:     3. Expand a continuation vanilla leaf beam  $(\hat{S}_{1:t-1}^m, X_{1:t})$ , compute its score, and
14:     4. maintain the same ID and the same parent ID of the original beam.
15:   end for
16:   end procedure
17:   for the  $m$ th group of vanilla leaf beams with ending state sequence  $A_m$  (in parallel) do
18:     procedure MARGINALIZING
19:       1. Sort the parent ID of all vanilla leaf beams, and
20:       2. for leaf beams sharing the same parent ID, check if they also share the same last state
21:       3. Merge the redundant vanilla leaf beams as described in Chapter 3.1.1.
22:       4. Promote the non-redundant vanilla leaf beams as leaf beams.
23:     end procedure
24:     procedure PRUNING
25:       1. Promote the highest-scored leaf beam as the new beam  $(\hat{S}_{1:t}^m, X_{1:t})$ .
26:     end procedure
27:   end for
28: end for
29: procedure BACKWARDS-TRACKING
30: 1. Select the highest-scored beam  $(\hat{S}_{1:T}^m, X_{1:T}) = \operatorname{argmax} \bar{\chi}_T(\hat{S}_{1:T}^m)$ .
31: 2. Back trace to the ancestor beam pinpointed by the parent ID of the selected beam.
32: 3. Concatenating the recorded last outer states in the parent beam.
33: 4. If the timestamp in the parent ID is 0, end the procedure, otherwise,
34: 5. make the parent beam the selected beam and return to 2.
35: end procedure

```

References

- [1] Søren Riis. *Hidden Markov models and neural networks for speech recognition*. Technical University of Denmark [Department of Mathematical Modeling], 1998.
- [2] Mark Gales and Steve Young. *Application of Hidden Markov Models in Speech Recognition*. Now Foundations and Trends, 2008.
- [3] Ya-Ti Peng, Ching-Yung Lin, Ming-Ting Sun, and Kun-Cheng Tsai. Healthcare audio event classification using hidden Markov models and hierarchical hidden Markov models. In *2009 IEEE International conference on multimedia and expo*, pages 1218–1221. IEEE, 2009.
- [4] Katherine Heller, Yee Whye Teh, and Dilan Gorur. Infinite hierarchical hidden Markov Models. In David van Dyk and Max Welling, editors, *Proceedings of the Twelfth International Conference on Artificial Intelligence and Statistics*, volume 5 of *Proceedings of Machine Learning Research*, pages 224–231, Hilton Clearwater Beach Resort, Clearwater Beach, Florida USA, 16–18 Apr 2009. PMLR.
- [5] S. E. Levinson. Continuously variable duration hidden Markov models for automatic speech recognition. *Computer Speech and Language*, 1:29–45, 1986.
- [6] Timo Adam, Christopher A Griffiths, Vianey Leos-Barajas, Emily N Meese, Christopher G Lowe, Paul G Blackwell, David Righton, and Roland Langrock. Joint modelling of multi-scale animal movement data using hierarchical hidden Markov models. *Methods in Ecology and evolution*, 10(9):1536–1550, 2019.
- [7] Nam Thanh Nguyen, Dinh Q Phung, Svetha Venkatesh, and Hung Bui. Learning and detecting activities from movement trajectories using the hierarchical hidden Markov model. In *2005 IEEE Computer Society Conference on Computer Vision and Pattern Recognition (CVPR’05)*, volume 2, pages 955–960. IEEE, 2005.
- [8] Svebor Karaman, Jenny Benois-Pineau, Vladislavs Dovgalecs, Rémi Mégret, Julien Pinquier, Régine André-Obrecht, Yann Gaëstel, and Jean-François Dartigues. Hierarchical hidden Markov Model in detecting activities of daily living in wearable videos for studies of dementia. *Multimedia tools and applications*, 69:743–771, 2014.
- [9] Parviz Asghari, Elnaz Soleimani, and Ehsan Nazerfard. Online human activity recognition employing hierarchical hidden Markov models. *Journal of Ambient Intelligence and Humanized Computing*, 11:1141–1152, 2020.
- [10] Miten Jain, Hugh E. Olsen, Benedict Paten, and Mark Akeson. The Oxford Nanopore MinION: Delivery of nanopore sequencing to the genomics community. *Genome Biology*, 17, 12 2016.
- [11] Xuechun Xu, Nayanika Bhalla, Patrik Ståhl, and Joakim Jaldén. Lokatt: A hybrid DNA nanopore basecaller with an explicit duration hidden Markov model and a residual LSTM network. *bioRxiv*, 2022.
- [12] Evan D. Tarbell and Tao Liu. Hmrratac: a hidden Markov Modeler for ATAC-seq. *Nucleic acids research*, 47:e91, 9 2019.
- [13] Shai Fine, Yoram Singer, and Naftali Tishby. The hierarchical hidden Markov Model: Analysis and Applications. *Machine Learning*, 32, 1998.
- [14] Kevin P Murphy and Mark Paskin. Linear-time inference in hierarchical HMMs. In *Advances in Neural Information Processing Systems*, volume 14. MIT Press, 2001.
- [15] Churbanov Alexander, Baribault Carl, and Winters-Hilt Stephen. Duration learning for analysis of nanopore ionic current blockades. *BMC Bioinformatics*, 8, 11 2007.
- [16] Broňa Brejová, Daniel G. Brown, and Tomáš Vinař. The most probable labeling problem in HMMs and its application to bioinformatics. In *Algorithms in Bioinformatics*, pages 426–437, Berlin, Heidelberg, 2004. Springer Berlin Heidelberg.
- [17] Haotian Teng, Minh Duc Cao, Michael B. Hall, Tania Duarte, Sheng Wang, and Lachlan J.M. Coin. Chiron: translating nanopore raw signal directly into nucleotide sequence using deep learning. *GigaScience*, 2018.
- [18] Oxford Nanopore Technologies plc. Nanoporetech/Bonito: A Pytorch basecaller for Oxford Nanopore reads. <https://github.com/nanoporetech/bonito>, February 2020.
- [19] Akira Hayashi, Kazunori Iwata, and Nobuo Suematsu. Marginalized Viterbi algorithm for hierarchical hidden Markov models. *Pattern Recognition*, 46:3452–3459, 12 2013.
- [20] Qiang Guo, Fenglei Wang, Jun Lei, Dan Tu, and Guohui Li. Convolutional feature learning and hybrid CNN-HMM for scene number recognition. *Neurocomputing*, 184:78–90, 2016. RoLoD: Robust Local Descriptors for Computer Vision 2014.
- [21] Qiujia Li, Chao Zhang, and Philip C. Woodland. Combining hybrid DNN-HMM ASR systems with attention-based models using lattice rescoring. *Speech Communication*, 147:12–21, 2023.

- [22] Defense Technical Information Center. DTIC ADA049288: Speech understanding systems. Summary of results of the five-year research effort at Carnegie-Mellon University. 1977.
- [23] Volker Steinbiss, Bach-Hiep Tran, and Hermann Ney. Improvements in beam search. In *Third international conference on spoken language processing*, 1994.
- [24] Monalisa Mazumdar, Mun-Ho Jeong, and Bum-Jae You. An online optimal path decoder for HMM towards connected hand gesture recognition. *IFAC Proceedings Volumes*, 41(2):736–741, 2008. 17th IFAC World Congress.
- [25] Heng Zhang, Xiang-Dong Zhou, and Cheng-Lin Liu. Keyword spotting in handwritten chinese documents using semi-Markov conditional random fields. *Engineering Applications of Artificial Intelligence*, 58:49–61, 2017.
- [26] Xiaoyuan Zhu and Changhe Yuan. Hierarchical beam search for solving most relevant explanation in Bayesian networks. *Journal of Applied Logic*, 22:3–13, 2017. SI:Uncertain Reasoning.
- [27] K. E. Batcher. Sorting networks and their applications. In *Proceedings of the April 30–May 2, 1968, Spring Joint Computer Conference*, AFIPS '68 (Spring), page 307–314, New York, NY, USA, 1968. Association for Computing Machinery.
- [28] ShunZheng Yu and Hisashi Kobayashi. Practical implementation of an efficient forward-backward algorithm for an explicit-duration hidden Markov model. *IEEE Transactions on Signal Processing*, 54(5):1947–1951, 2006.
- [29] Yi-Jian Wu, Hisashi Kawai, Jinfu Ni, and Ren-Hua Wang. Discriminative training and explicit duration modeling for HMM-based automatic segmentation. *Speech Communication*, 47(4):397–410, 2005.
- [30] Shun Zheng Yu. Hidden semi-Markov models. *Artificial Intelligence*, 174:215–243, 2 2010.
- [31] Gonzalo Navarro. A guided tour to approximate string matching. *ACM Computing Surveys*, 33, 04 2000.
- [32] Peter JA Cock, Tiago Antao, Jeffrey T Chang, Brad A Chapman, Cymon J Cox, Andrew Dalke, Iddo Friedberg, Thomas Hamelryck, Frank Kauff, Bartek Wilczynski, et al. Biopython: freely available Python tools for computational molecular biology and bioinformatics. *Bioinformatics*, 25(11):1422–1423, 2009.
- [33] NVIDIA, Péter Vingelmann, and Frank H.P. Fitzek. Cuda, release: 10.2.89, 2020.
- [34] Heng Li. Minimap2: Pairwise alignment for nucleotide sequences. *Bioinformatics*, 34:3094–3100, 2018.
- [35] Alex Graves, Santiago Fernández, Faustino Gomez, and Jürgen Schmidhuber. Connectionist temporal classification: Labelling unsegmented sequence data with recurrent neural networks. volume 2006, pages 369–376, 01 2006.

Appendix A

We will derive (5) by induction using the two-level HHMM described in chapter 2, where we divided the inner state space into the continuation set \mathbb{S}_c^2 , and the end set \mathbb{S}_e^2 . We let $\mathbb{B}_t(\hat{S}_{1:l})$ be the joint time-aligned sequences $S_{1:t} = (S_{1:t}^1, S_{1:t}^2)$ that map to a sequence-aligned outer state sequence $\hat{S}_{1:l}$. The objective of the decoding problem essentially is to, given an observation sequence $X_{1:t}$, compute or approximate the metric

$$P(X_{1:t}, \hat{S}_{1:l}) = \sum_{S_{1:t} \in \mathbb{B}_t(\hat{S}_{1:l})} P(X_{1:t}, S_{1:t})$$

for all candidate sequences $\hat{S}_{1:L}$ and select the maximum of these sequences.

Let $\chi_t(\hat{S}_{1:l}, i)$ denotes the probability of the sequence-aligned states $\hat{S}_{1:l}$ with a specific current inner state $S_t^2 = i$ with $i \in \mathbb{S}^2$ such that

$$\chi_t(\hat{S}_{1:l}, i) = \sum_{S_{1:t} \in \mathbb{B}_t(\hat{S}_{1:l}), S_t^2 = i} P(S_{1:t}, X_{1:t}). \quad (8)$$

Further, let $\mathbb{B}_t^c(\hat{S}_{1:l})$ be given by

$$\mathbb{B}_t^c(\hat{S}_{1:l}) = \{S_{1:t} \mid S_{1:t-1} \in \mathbb{B}_{t-1}(\hat{S}_{1:l-1}), S_{t-1} = (\hat{S}_{l-1}, j)\}$$

if $j \in \mathbb{S}_c^2$, and

$$\mathbb{B}_t^c(\hat{S}_{1:l}) = \{S_{1:t} \mid S_{1:t-1} \in \mathbb{B}_{t-1}(\hat{S}_{1:l}), S_{t-1} = (\hat{S}_l, k)\}$$

if $k \in \mathbb{S}_e^2$. By construction, we have $\mathbb{B}_t(\hat{S}_{1:l}) = \mathbb{B}_t^c(\hat{S}_{1:l}) \cup \mathbb{B}_t^e(\hat{S}_{1:l})$ while $\mathbb{B}_t^c(\hat{S}_{1:l}) \cap \mathbb{B}_t^e(\hat{S}_{1:l}) = \emptyset$, which implies that

$$\chi_t(\hat{S}_{1:l}, i) = \sum_{S_{1:t} \in \mathbb{B}_t^c(\hat{S}_{1:l}), S_t^2 = i} P(S_{1:t}, X_{1:t}) + \sum_{S_{1:t} \in \mathbb{B}_t^e(\hat{S}_{1:l}), S_t^2 = i} P(S_{1:t}, X_{1:t})$$

Note now that for any $S_{1:t} \in \mathbb{B}_t(\hat{S}_{1:l})$, we can obtain

$$\begin{aligned} & P(S_{1:t}, X_{1:t}) \\ &= P(S_t, X_t, S_{1:t-1}, X_{1:t-1}) \\ &= P(S_t, X_t \mid S_{1:t-1}, X_{1:t-1}) P(S_{1:t-1}, X_{1:t-1}), \end{aligned}$$

and use the HHMM assumption to conclude that

$$P(S_t, X_t \mid S_{1:t-1}, X_{1:t-1}) = P(S_t, X_t \mid S_{t-1}).$$

This implies that

$$\begin{aligned} \chi_t(\hat{S}_{1:l}, i) &= \sum_{S_{1:t} \in \mathbb{B}_t^c(\hat{S}_{1:l}), S_t^2 = i} P(S_{1:t}, X_{1:t}) + \sum_{S_{1:t} \in \mathbb{B}_t^e(\hat{S}_{1:l}), S_t^2 = i} P(S_{1:t}, X_{1:t}) \\ &= \sum_{S_{1:t} \in \mathbb{B}_t^c(\hat{S}_{1:l}), S_t^2 = i} P(S_t, X_t \mid S_{t-1}) P(X_{1:t-1}, S_{1:t-1}) \\ &\quad + \sum_{S_{1:t} \in \mathbb{B}_t^e(\hat{S}_{1:l}), S_t^2 = i} P(S_t, X_t \mid S_{t-1}) P(X_{1:t-1}, S_{1:t-1}) \\ &= \sum_{j \in \mathbb{S}_c^2} P(S_t, X_t \mid S_{t-1} = (\hat{S}_{l-1}, j)) \sum_{S_{1:t-1} \in \mathbb{B}_{t-1}(\hat{S}_{1:l-1}), S_{t-1}^2 = j} P(S_{1:t-1}, X_{1:t-1}) \\ &\quad + \sum_{k \in \mathbb{S}_e^2} P(S_t, X_t \mid S_{t-1} = (\hat{S}_l, k)) \sum_{S_{1:t-1} \in \mathbb{B}_{t-1}(\hat{S}_{1:l}), S_{t-1}^2 = k} P(S_{1:t-1}, X_{1:t-1}) \\ &= \sum_{j \in \mathbb{S}_c^2} P(S_t, X_t \mid S_{t-1} = (\hat{S}_{l-1}, j)) \chi_{t-1}(\hat{S}_{1:l-1}, j) \\ &\quad + \sum_{k \in \mathbb{S}_e^2} P(S_t, X_t \mid S_{t-1} = (\hat{S}_l, k)) \chi_{t-1}(\hat{S}_{1:l}, k). \end{aligned}$$

In other words, one can recursively compute $\chi_t(\hat{S}_{1:l}, i)$ for any sequence $\hat{S}_{1:l}$ and the inner state i from the values of χ_{t-1} .